

Ultra-High Quantum Dot Color Conversion in Graphene-Connected Nanorod Micro-LEDs via Non-Radiative Energy Transfer and Localized

Downloaded from: https://research.chalmers.se, 2025-11-06 18:41 UTC

Citation for the original published paper (version of record):

Fang, A., Li, Q., Liu, J. et al (2025). Ultra-High Quantum Dot Color Conversion in Graphene-Connected Nanorod Micro-LEDs via Non-Radiative Energy Transfer and Localized Surface Plasmon Resonance. Laser and Photonics Reviews, 19(20). http://dx.doi.org/10.1002/lpor.202500389

N.B. When citing this work, cite the original published paper.

research.chalmers.se offers the possibility of retrieving research publications produced at Chalmers University of Technology. It covers all kind of research output: articles, dissertations, conference papers, reports etc. since 2004. research.chalmers.se is administrated and maintained by Chalmers Library

REVIEWS

www.lpr-journal.org

Ultra-High Quantum Dot Color Conversion in Graphene-Connected Nanorod Micro-LEDs via Non-Radiative Energy Transfer and Localized Surface Plasmon Resonance

Aoqi Fang, Qingqing Li, Jixin Liu, Zaifa Du, Penghao Tang, Hao Xu, Rongjing Wang, Yiyang Xie, Jibin Song, Qun Yan, Weiling Guo,* and Jie Sun*

In the field of quantum dot (QD)-based micro-light-emitting diode (µLED) full-color display technology, achieving high color conversion efficiency (CCE) is one of the key performance indicators. In this work, a µLED architecture is presented that incorporates an optimized nanorod array, with QDs and nanogapped gold nanoparticles (AuNNPs) embedded in the inter-rod gaps. By harnessing non-radiative energy transfer (NRET) and localized surface plasmon resonance (LSPR), the absorption and utilization of quantum well (QW) energy by the QDs are significantly enhanced. To ensure efficient current spreading and uniform light emission, graphene is employed as a transparent conductive layer to interconnect the nanorods. As graphene can transfer photogenerated carriers to the QDs, enhancing their quantum yield, it is also introduced as an intermediate insertion layer and support layer, allowing the integration of a second layer of QDs and AuNNPs on the light-emitting surface. This design maintains the electrical performance of the nanorod µLED while achieving ultra-high CCE. Experimental results demonstrate that the proposed µLED with nanorod structures and AuNNPs achieves a maximum CCE of 94%, representing a 102% improvement compared to conventional planar µLEDs. These findings offer promising insights for advancing high-performance, full-color µLED display technologies through nanoscale engineering.

1. Introduction

The challenge of achieving full-color display remains a key factor limiting the widespread adoption of Micro Light-Emitting Diodes (µLEDs) in the application market.[1-3] While mass transfer technology is suitable for the large-scale fabrication of µLED full-color displays, it requires extremely high alignment precision and transfer yield, which leads to high production costs. These limitations make mass transfer less advantageous, particularly for small-screen µLED fullcolor displays. [4–7] Alternative approaches include the three-primary-color stacking method and quantum dot (QD) color conversion technology. The three-primarycolor stacking method vertically bonds red, green, and blue $\mu LEDs$ within the same pixel area. However, this poses significant challenges to fabrication processes and bonding precision. Moreover, vertical stacking results in severe optical crosstalk among the three colors, leading

A. Fang, J. Liu, P. Tang, H. Xu, R. Wang, Y. Xie, W. Guo Key Laboratory of Optoelectronics Technology Beijing University of Technology

Beijing 100124, China E-mail: guoweiling@bjut.edu.cn

The ORCID identification number(s) for the author(s) of this article can be found under https://doi.org/10.1002/lpor.202500389

© 2025 The Author(s). Laser & Photonics Reviews published by Wiley-VCH GmbH. This is an open access article under the terms of the Creative Commons Attribution-NonCommercial-NoDerivs License, which permits use and distribution in any medium, provided the original work is properly cited, the use is non-commercial and no modifications or adaptations are made.

DOI: 10.1002/lpor.202500389

Q. Li
College of Chemistry
Chemical Engineering and Materials Science
Collaborative Innovation Center of Functionalized Probes for Chemical
Imaging in Universities of Shandong
Key Laboratory of Molecular and Nano Probes
Ministry of Education
Shandong Normal University
Jinan 250014, China
O. Yan, J. Sun

Fujian Science and Technology Innovation Laboratory for Optoelectronic Information of China, and College of Physics and Information Engineering

Fuzhou University
Fuzhou 350100, China
E-mail: jie.sun@fzu.edu.cn

www.advancedsciencenews.com

www.lpr-journal.org

to suboptimal display quality.[8-10] Consequently, researchers have turned their attention to QD-based color conversion technology. In QD full-color display technology, techniques such as photolithography or inkjet printing are employed to pattern red and green QDs (or red, green, and blue QDs) as color conversion media. This enables full-color display in μLED arrays with blue or ultraviolet light sources.[11-15] QD-based full-color display technology offers lower fabrication complexity and is compatible with large-scale manufacturing. However, its two major shortcomings are low luminous efficiency and suboptimal color conversion efficiency (CCE) due to QD material limitations.[16,17] Typically, a thicker QD layer is used to achieve higher CCE. However, QDs inherently possess numerous defect states, and a significant portion of energy is lost during photon down-conversion from high-energy states to lower-energy states. A thicker QD layer further exacerbates this issue, leading to a substantial decrease in emission intensity after conversion.^[18-21] Thus, it is crucial to strike a balance between CCE and luminous efficiency by developing a QD- μ LED with ultra-high CCE and minimal luminous efficiency loss, which would greatly advance the application of QDs in µLED full-color displays. Research indicates that nonradiative energy transfer (NRET), unlike traditional fluorescencebased conversion, enables direct energy transfer from the quantum well (QW) to the QD through dipole coupling. This process bypasses photon emission and reabsorption in the QW-QD system, thereby minimizing energy losses and significantly enhancing CCE. $^{\hbox{\scriptsize [22-26]}}$ In addition, localized surface plasmon resonance (LSPR) can substantially boost the emission efficiency of luminescent materials, enhancing QD radiative recombination and quantum yield.[27-30] In our previous work, we combined nanostructures and nanomaterials to integrate NRET and LSPR mechanisms. By suppressing non-radiative recombination within QDs, we effectively improved their absorption and emission efficiencies, thereby enhancing the CCE of QD-based µLEDs. Furthermore, we found that plasmon resonances with peak absorption wavelengths matching the QD emission wavelength provided the greatest enhancement in CCE.[31]

In this paper, we fabricated a size-optimized nanorod (NR) array structure on the light-emitting mesa of a blue μLED with an emission wavelength of 450 nm. The nanorods have a diameter of 500 nm, and the gaps between them measure 350 nm. QDs mixed with nanogapped gold nanoparticles (AuNNPs) were filled into the nanorod gaps, and the absorption resonance peak of the AuNNPs is tuned to match the emission wavelength of the QDs. The nanorod structure offers two key advantages. First, it

J. Sun
Quantum Device Physics Laboratory
Department of Microtechnology and Nanoscience
Chalmers University of Technology
Gothenburg 41296, Sweden
Z. Du
School of Physics and Electronic Information
Weifang University
Weifang 261061, China
J. Song
State Key Laboratory of Chemical Resource Engineering
College of Chemistry
Beijing University of Chemical Technology
Beijing 10010, China

mitigates the quantum-confined Stark effect (QCSE) induced by piezoelectric and spontaneous polarization in InGaN/GaN materials. Second, it facilitates direct or ultra-close contact between the QDs and the QWs, enabling NRET. This significantly enhances the energy utilization and color conversion efficiency of the QDs. The AuNNPs play a critical role in generating LSPR. Through the LSPR-induced ultrahigh localized electromagnetic field around the surface of the AuNNPs, the radiative recombination efficiency of carriers within the QDs can be enhanced, further improving the CCE of the QDs. To ensure efficient current spreading and uniform light emission in the NR-µLED structure, we transferred a graphene layer onto the light-emitting mesa as a transparent conductive layer. Furthermore, to efficiently collect and utilize the blue light emitted from the QWs at the top of the nanorods, the second layer of QD/AuNNP mixture was integrated onto the graphene. According to the theory of band bending, graphene can transport photogenerated carriers to the QDs, thereby enhancing their radiative recombination efficiency and quantum yield.[32,33] In this approach, graphene also functions as an inserted carrier transport layer, further enhancing the recombination efficiency of the QDs. Detailed optoelectronic performance measurement and simulation results demonstrate the significant effects of combining NRET, LSPR, and graphene in enhancing the CCE of QD-µLEDs, with the structure achieving a CCE exceeding 90%. Compared to traditional planar µLEDs with QDs (Plane-µLED-QD), the NR-µLED-QD-Au improves the CCE by over 100% while maintaining superior luminous efficiency.

2. Results

Figure 1 shows the fabrication process of the QD-based NR- μ LED that enhances the CCE through LSPR and NRET, more detailed fabrication process can be found in the Experimental section.

Figure 2a shows a scanning electron microscope (SEM) image of the NR-µLED we fabricated. Figure 2b,c illustrate the difference in the nanorod region before and after the graphene transfer. It can be observed that the morphology of the graphene layer remains intact, and as a transparent conductive layer, it effectively connects the individual nanorods. Figure 2d shows the visible light transmittance of the double-layer graphene formed by the two-step transfer. The transmittance at the LED emission wavelength (peak wavelength 450 nm) is 94%, and at the QD emission wavelength (peak wavelength 630 nm), the transmittance is 95%. The Raman spectra of monolayer graphene (transferred once) and double-layer graphene (formed by two transfers) show significant differences, as shown in Figure 2e. The peak full-width at half-maximum of the 2D peak and the ratio of the 2D peak to the G peak indicate that the original graphene is monolayer.^[34] Due to the two transfer steps, wrinkles or impurity contamination were inevitably introduced, resulting in slight defects in the double-layer graphene, but this is acceptable. The current-voltage characteristics shown in Figure 2f indicate that the NR-µLED with graphene as the transparent conductive layer has significantly lower conduction resistance. This suggests that graphene forms a good electrical contact with the top of the nanorods, effectively connecting the individual nanorods, and the reverse leakage current of the nanorods is also very low, comparable to the plane-µLED. This indicates that our sidewall treatment process is effective. The only drawback is that the NR-µLED with

186388989, 2025, 20, Downloaded from https://onlinelbrary.wiley.com/doi/10.1002/por.202500389 by Statens Beredning, Wiley Online Library on [05/11/2025]. Se the Terms and Conditions (https://onlinelbrary.wiley.com/terms-and-conditions) on Wiley Online Library for rules of use; OA arcicles are governed by the applicable Creative Commons. License 1865, 1

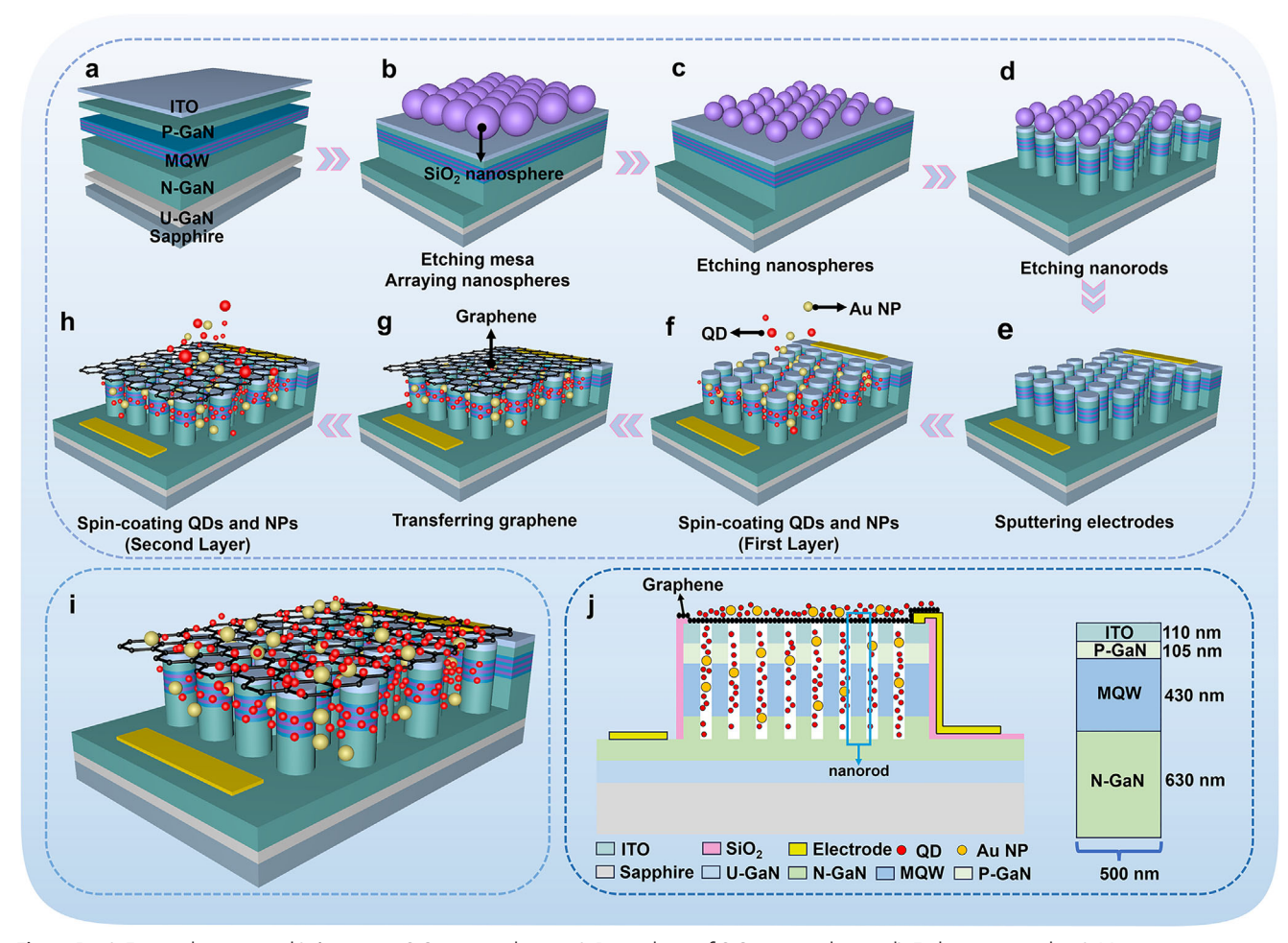


Figure 1. a) Epitaxial structure. b) Arranging SiO₂ nanospheres. c) Pre-etching of SiO₂ nanospheres. d) Etching nanorods. e) Magnetron sputtering of metal electrodes, f) Spin-coating the first layer of QD/AuNNP into the nanorod gaps. g) Transferring graphene, h) Spin-coating the second layer of QD/AuNNP on top of the nanorods. i) Final device structure, j) Cross-sectional structure of the device and schematic of a single nanorod.

graphene exhibits a forward leakage current of 1-2 mA, caused by partial damage and collapse of the graphene in some regions, which leads to contact between graphene and the nanorod sidewalls. The optical performance of the NR-µLED before and after graphene transfer also shows significant improvement, as shown in Figure 2g,h. Without the graphene transparent conductive layer, the nanorod regions of the NR-µLED are not able to conduct properly because the nanorods are not connected to each other, resulting in most of the mesa area not emitting light. This issue is resolved with the introduction of graphene. At a current of 10 mA, the electroluminescence (EL) intensity increases by 35%. While the nanorod structure can enhance light extraction efficiency, the light output power and EL intensity of the NR-µLED with the graphene conductive layer are still lower than those of the plane-µLED, mainly due to the loss of the active region area and the absorption of a small portion of light by the graphene. However, at low current densities, their performance is nearly identical, which is the operating current range for µLEDs. Furthermore, we observe a significant blue shift in the EL spectrum of the NR-µLED compared to the plane-µLED. Thus, we have made a detailed comparison of the peak wavelengths of the three

types of µLEDs at different currents, as shown in Figure 2i. At lower currents, the peak wavelength of the μLED exhibits a noticeable blue shift as the current increases. This is due to the built-in electric field caused by the strong polarization effect of the In-GaN/GaN multi-quantum wells (MQWs).[35] As the injected current becomes larger, the carrier lifetime is relatively long, and the carriers accumulate in the MQWs. The accumulated electrons and holes shield the built-in electric field, causing the peak wavelength to stabilize.^[36] The introduction of the nanorod structure alleviates the QCSE caused by the piezoelectric polarization between GaN and InGaN, so the peak wavelength of the NR- μ LED exhibits a blue shift compared to the plane-µLED.[37,38] There is also a slight difference in the peak wavelengths of NR-µLEDs with and without the graphene transparent conductive layer. Without graphene, the nanorod region cannot contribute to light emission, and the QCSE alleviation by the nanorods is limited. With graphene, the nanorods are fully connected, enabling light emission and causing a further blue shift in the peak wavelength.

Figure 3a,b illustrate the energy transfer mechanisms of NRET and LSPR, respectively. [26,39] When the QD is in close proximity to the QW (less than 10 nm) and exhibits high absorption at

18638899, 2025, 20, Downloaded from https://onlinelibrary.wiley.com/doi/10.1002/por.202500389 by Statens Beredning, Wiley Online Library on [05/11/2025], See the Terms and Conditions (https://onlinelibrary.wiley.com/terms-and-conditions) on Wiley Online Library for rules of use; OA articles are governed by the applicable Creative Commonsors.

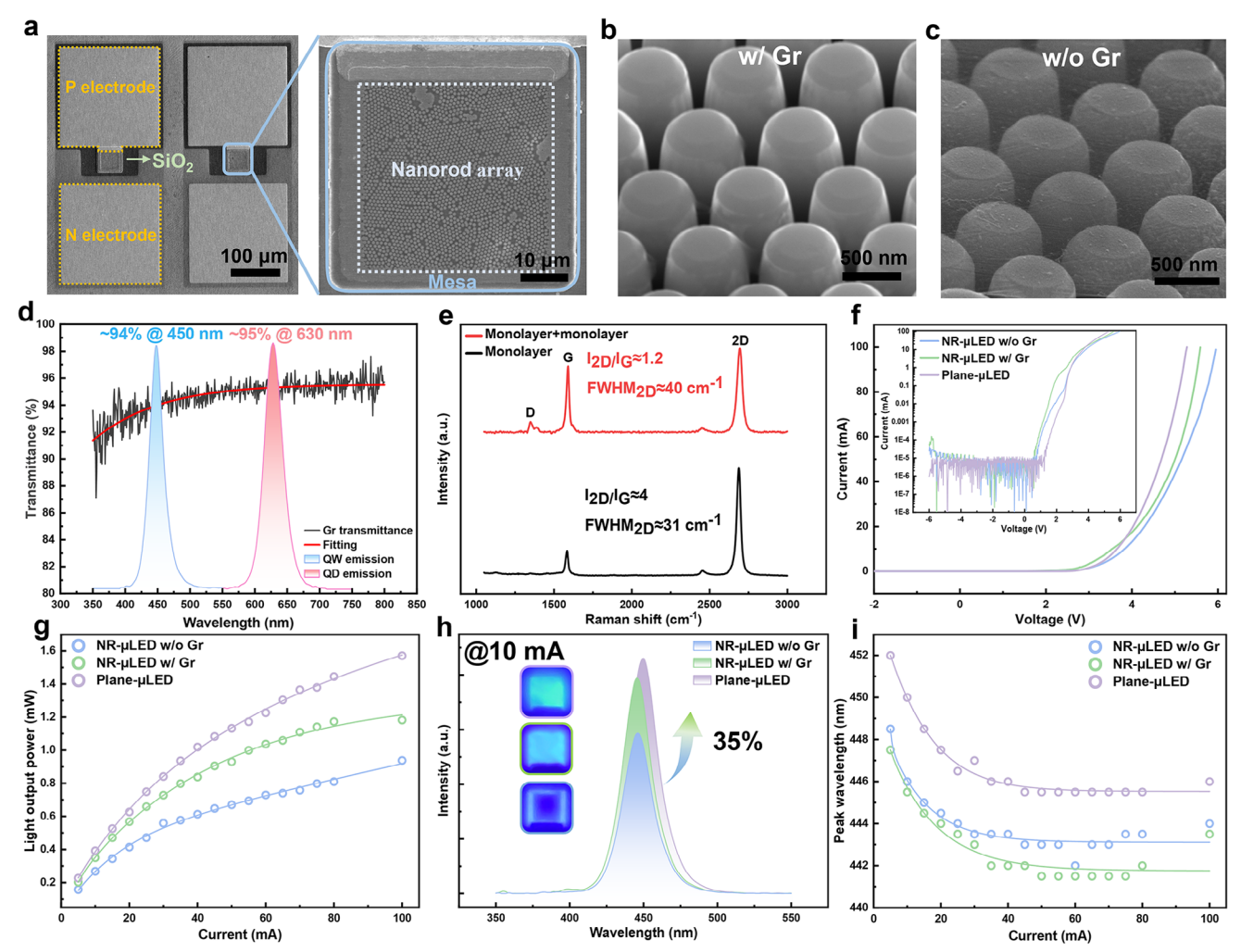


Figure 2. a) SEM image of the NR-μLED, with the enlarged view showing the light-emitting mesa region. b,c) Morphology of the nanorods before and after graphene transfer. d) Transmittance of the transferred graphene in the range of 350–800 nm. e) Raman spectra of graphene after one and two transfer steps. Comparison of the performance of NR-μLEDs with and without graphene transparent electrodes, as well as plane-μLEDs, including f) IV characteristics, g) light output power, h) EL spectra at a current of 10 mA, and i) peak wavelength.

the QW's emission wavelength, part of the exciton energy in the QW (the remaining energy either radiatively recombines to emit photons or is lost through non-radiative recombination) is transferred directly to the QD via dipole coupling. Upon energy transfer to the QD, intraband transitions occur immediately within the QD to prevent reverse transfer, followed by interband transitions that emit low-frequency photons.

Simultaneously, when AuNNP is in close proximity to QD (less than 100 nm) and its absorption peak highly overlaps with the QD emission wavelength, a strong electric field is generated around the AuNNP. This field can transfer energy to the QD via resonant coupling, enhancing the emission intensity of the QD. Additionally, excited electrons on the AuNNP surface may transfer to the conduction band or defect states of the QD, subsequently recombining radiatively with holes in the valence band to emit photons.

In Figure 3c, we explain the electron state modulation mechanism between QD and AuNNP. [40,41] The QD used are CdSe/ZnS core-shell structures with a work function of \approx 6 eV, while Au has a work function of \approx 4.5 eV. When AuNNP come into contact with

QDs, this work function difference causes electrons to transfer from Au to the QD, establishing a new common Fermi level. This process induces a downward band bending in the QD, causing electron accumulation near the QD-AuNNP interface. The electron accumulation alters the electronic state distribution within the QD, making it easier for electrons to transition to the conduction band and defect levels, thereby promoting radiative recombination. Furthermore, electrons in AuNNP can be excited by surface plasmon waves to states above the conduction band edge of the QD. These excited electrons can transition more efficiently into the conduction band and defect states of the QD, further enhancing bandgap and defect emissions, ultimately increasing the quantum yield of the QD.

Figure 4a–d shows the TEM images and particle size distribution of AuNNPs and QDs, while the structure of AuNNPs is presented in Figure 4e. The detailed fabrication steps are provided in the supporting information. The nanogap structure enables AuNNPs to achieve larger absorption wavelengths even at small diameters, ensuring that the absorption peak of AuNNPs

18638899, 2025, 20, Downloaded from https://onlinelibrary.wiley.com/doi/10.1002/lpor.202500389 by States Beredning, Wiley Online Library on [05/11/2025]. See the Terms and Conditions (https://onlinelibrary.wiley.com/terms-and-conditions) on Wiley Online Library for rules of use; OA articles are governed by the applicable Creative Commons

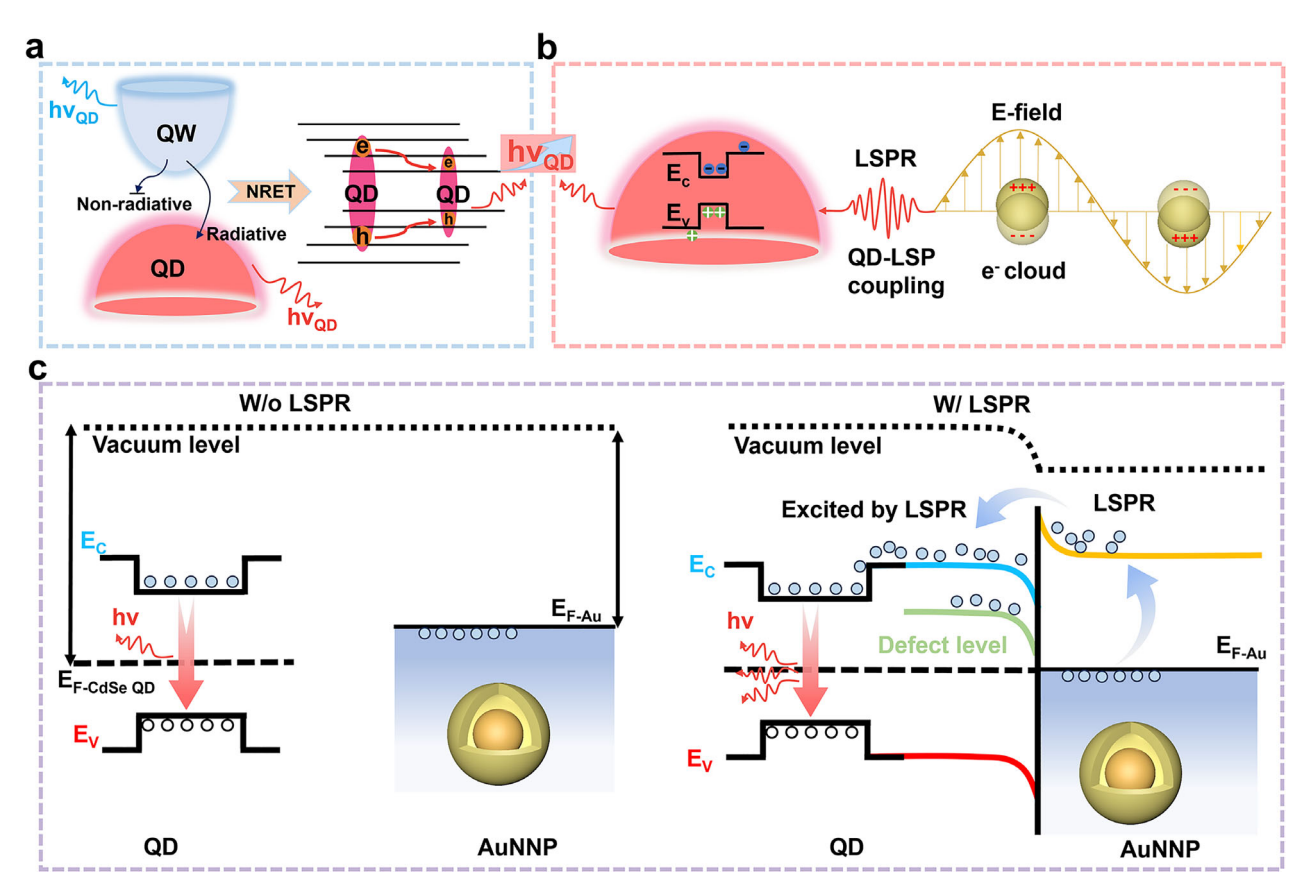


Figure 3. a) Energy transfer pathway between QW and QD in NRET. b) Physical mechanism of LSPR. c) Schematic of the band structure of AuNNP and CdSe QD before and after LSPR.

matches the emission band of QDs, which facilitates the occurrence of LSPR. Figure 4f depicts the absorption spectra of AuN-NPs and QDs, where the QDs exhibit strong absorption in the emission band of QWs. This characteristic allows QDs to efficiently absorb high-energy photons emitted by QWs and convert them into low-energy photon emissions while maintaining smooth and efficient NRET. Additionally, the absorption wavelength of AuNNPs is closely aligned with the emission band of QDs, satisfying one of the prerequisites for LSPR. Electromagnetic simulations of QD-Au interactions, shown in Figure 4g, reveal a significant enhancement in the electric field intensity when QDs are in close proximity to AuNNPs, confirming the feasibility of enhancing QDs emission via LSPR. In the supporting information, we conducted electromagnetic simulations to investigate the relationship between the distance between the QDs and the NPs and the resulting overall electric field intensity (Figure S4, Supporting Information). Further characterization through TRPL and PL spectra of QDs with and without AuNNPs reveals that the coupling between QDs and AuNNPs via LSPR results in shorter PL decay times for QDs mixed with AuNNPs (Figure 4h), indicating improved radiative recombination efficiency of photogenerated carriers within QDs. As shown in Figure 4i, the PL intensity of QD-AuNNP mixture demonstrates a notable 35% enhancement.

Figure 5a,b shows SEM images of the nanorods before and after being filled with QD/AuNNPs. From the SEM images and

EDS spectra analysis, it is evident that the QDs have uniformly infiltrated the gaps between the nanorods, while the tops of the nanorods remain relatively clean. The SEM image in Figure 5c clearly shows that the nanorods are fully encapsulated by the QDs/AuNNPs mixture, with virtually no visible residue on the tops of the nanorods. This ensures effective electrical contact between the graphene and the nanorods, allowing the nanorod regions to illuminate properly. To investigate the effects of the nanorod structure and AuNNP on the QW and QD, six different configurations were designed, as illustrated in Figure 5d. From the TRPL spectra of the QW shown in Figure 5e, it can be observed that the introduction of nanorods accelerates the PL decay of the QW, indicating enhanced carrier recombination efficiency. This is attributed to the nanorod structure alleviating piezoelectric polarization in InGaN/GaN, thereby mitigating the QCSE. The PL spectra comparison in Figure 5g between planar and nanorod structures further confirms this improvement, as the PL intensity of the nanorod structure is significantly higher, validating the successful enhancement of QW optical performance by the nanorods. When QDs are incorporated into the nanorods, NRET provides an additional energy transfer pathway for carriers in the QW, leading to faster carrier decay rates and shorter decay times. Moreover, when the QD/AuNNP mixture is introduced into the nanorod gaps, the LSPR effect of AuNNPs enhances the radiative recombination efficiency within the QDs, further boosting the NRET efficiency. This results in an even shorter carrier

18638899, 2025, 20, Downloaded from https://onlinelibrary.wiley.com/doi/10.1002/lpor.202500389 by States Beredning, Wiley Online Library on [05/11/2025]. See the Terms and Conditions (https://onlinelibrary.wiley.com/terms-and-conditions) on Wiley Online Library for rules of use; OA articles are governed by the applicable Creative Commons

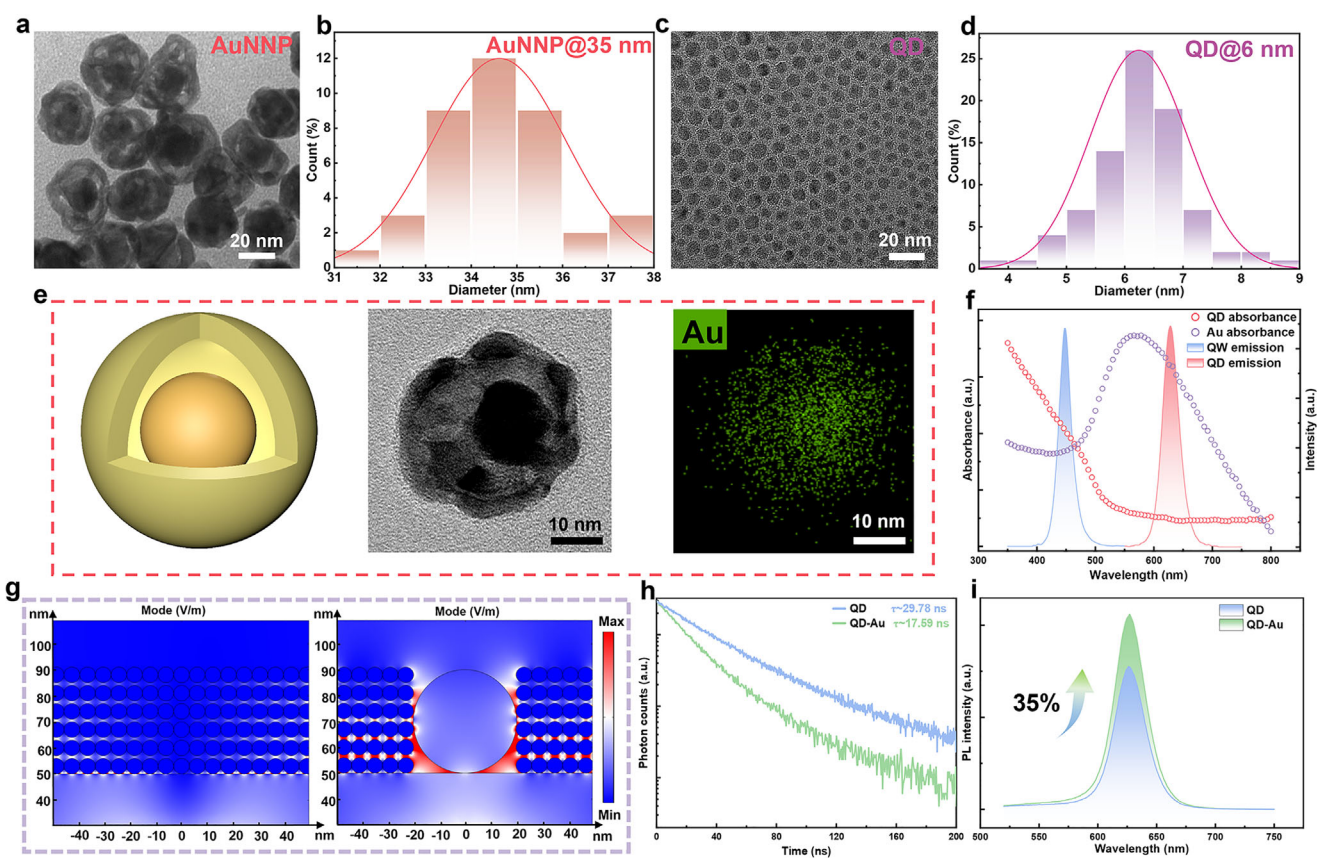


Figure 4. a,b) TEM images of AuNNPs and their size distribution. c,d) TEM images of QDs and their size distribution. e) Structural schematic of an AuNNP, along with a TEM image of a single AuNNP and its corresponding energy dispersive spectrometer (EDS) spectrum. f) Absorption spectra of QDs and AuNNPs. g) Comparison of electric field distribution in electromagnetic simulations for QDs without and with AuNNPs. h) PL spectra and i) TRPL spectra of QDs with and without AuNNPs.

decay time in the QW. The NRET efficiency can be calculated using the Equation (1): $^{[26,42]}$

$$\eta_{\rm ET} = \frac{\tau_{\rm ET}^{-1}}{\tau_{\rm ET}^{-1} + \tau_{\rm QW}^{-1}} \tag{1}$$

where $au_{\rm ET}$ and $au_{\rm OW}$ represent the PL decay times of the QW with and without NRET, respectively. Calculations show that the nonradiative energy transfer efficiency of NR-QD is 53%. With the addition of AuNNPs, the presence of LSPR increases the NRET efficiency of NR-QD-Au to 60%, representing an improvement of over 13%. Figure 5f presents the PL decay times of QDs in different structures. The nanorod structure enables direct or closerange interaction between QDs and QWs, introducing the NRET mechanism. This allows the energy of carriers in the QW to transfer directly into the QD for radiative recombination, bypassing the emission and absorption steps of traditional radiative energy transfer. Consequently, carrier recombination within the QD becomes more direct and faster, resulting in significantly shorter PL decay times in the nanorod structure compared to the planar structure. When AuNNPs are incorporated, the LSPR effect enhances the radiative recombination efficiency within the QDs, leading to even faster carrier decay rates and shorter PL decay times. This trend is also reflected in the PL spectra of QDs shown in Figure 5h, where the combined effects of the nanorod structure and LSPR significantly enhance the PL intensity of the QDs.

Figure 6a illustrates the schematic of two QD layers, one with and one without a graphene insertion layer. When a graphene insertion layer is introduced into the QD layer, as shown in Figure 6b, the PL spectrum of the QDs is enhanced. Furthermore, in Figure 6c, the PL decay lifetime of the QDs decreases from 18 to 10 ns, indicating an increase in the number of internal carriers and an acceleration of radiative recombination within the QDs. The electromagnetic simulation in Figure 6d reveals a significant enhancement in the electric field intensity within the QD region when the graphene insertion layer is present. The band diagram in Figure 6e explains this phenomenon. ^[32,33] Due to the lower work function of graphene compared to that of CdSe QDs, a band bending occurs at the graphene-QD interface, this results in the transfer of photoexcitation carriers from graphene to the QDs. According to the Equation (2):

$$R_{rad} = B \times n \times p \tag{2}$$

where R_{rad} is the radiative recombination rate, B is the radiative recombination coefficient, n and p are the electron and hole concentrations respectively. This equation indicates that the radiative

18638899, 2025, 20, Downloaded from https://onlinelbtrary.wiley.com/doi/10.1002/por.202500389 by Statens Beredning, Wiley Online Library on [05/11/2025]. See the Terms and Conditions (https://onlinelbtrary.wiley.com/terms-and-conditions) on Wiley Online Library for rules of use; OA articles are governed by the applicable Creative Commons License

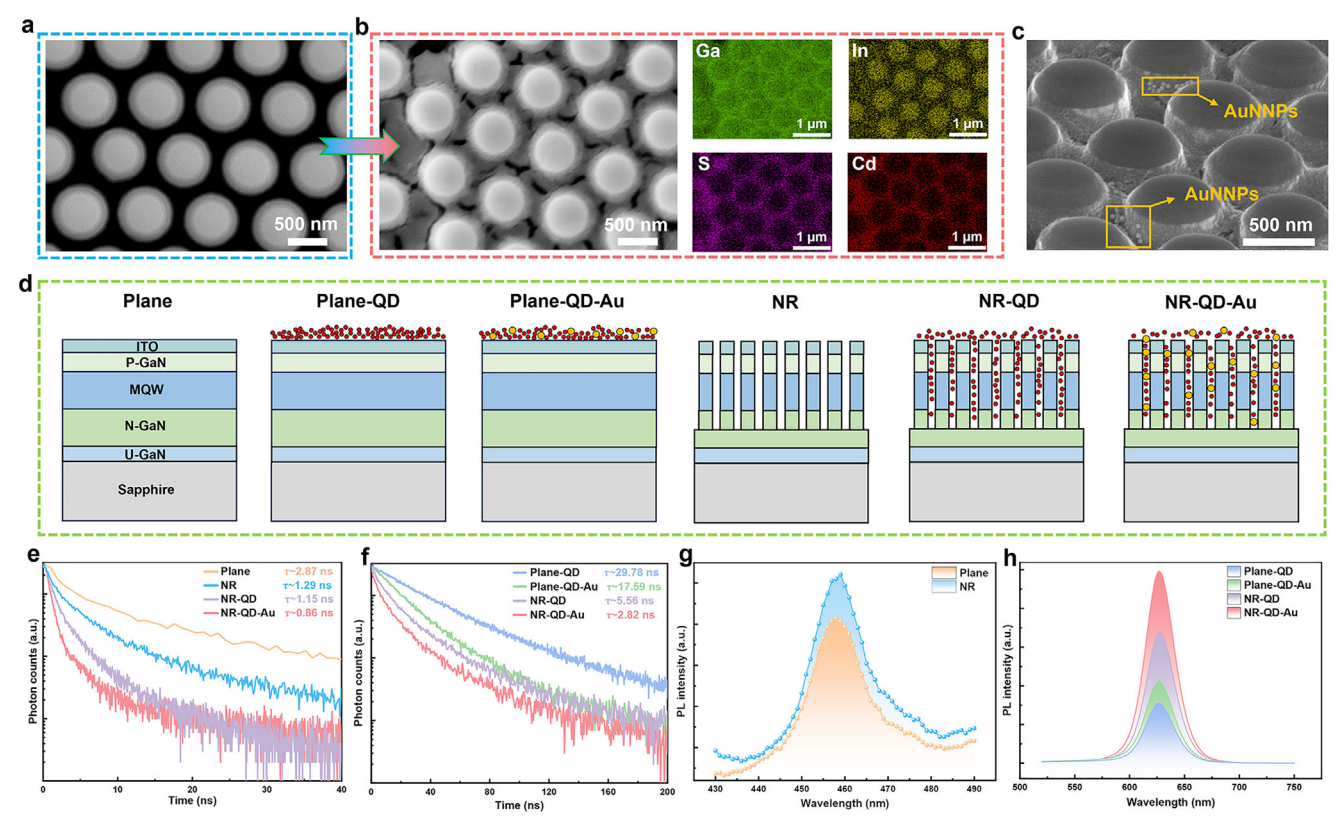


Figure 5. a) Top-view SEM image of the nanorods. b) Top-view SEM image of the nanorods after spin-coating with QD/AuNNPs and the corresponding EDS spectra. c) Cross-sectional SEM image of the nanorods after spin-coating with QD/AuNNPs. d) Schematic of six structures. TRPL spectra under 380 nm excitation e) QWs, f) QDs. g) PL spectra of QWs in planar and nanorod structures. h) PL spectra of QDs.

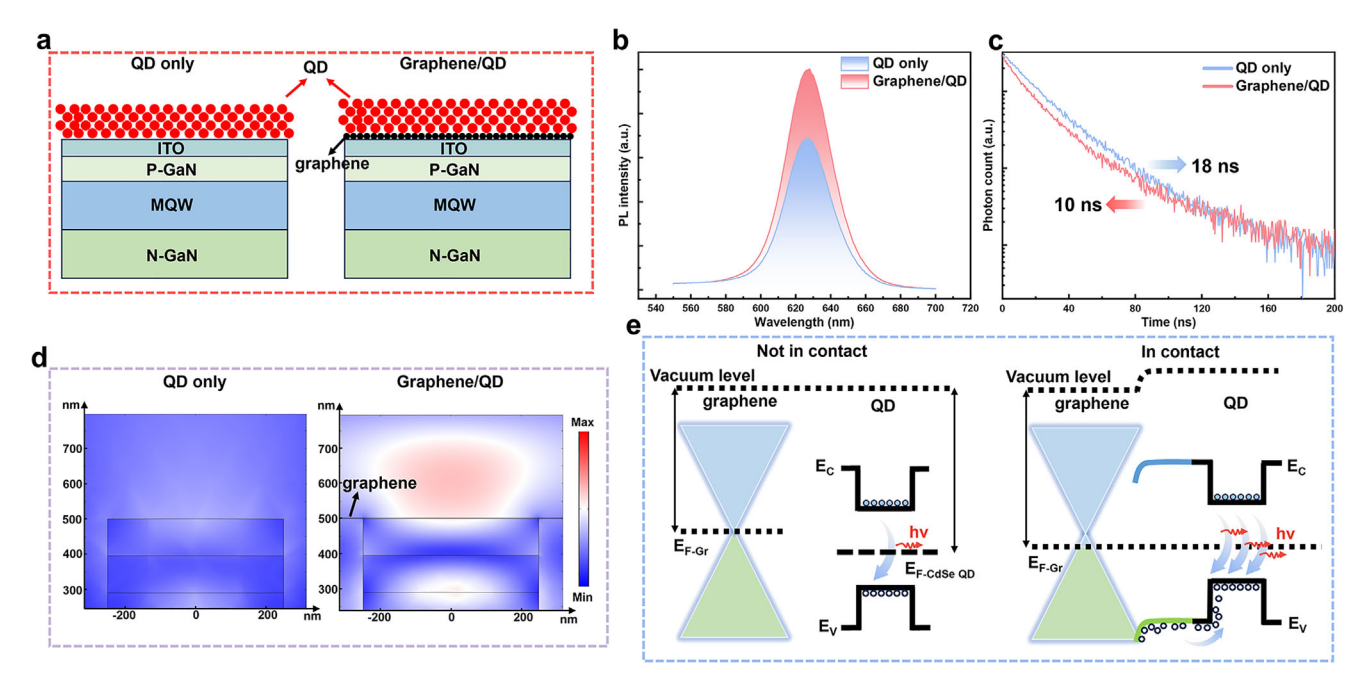


Figure 6. a) Schematic diagram of structures without and with graphene insertion layer. b,c,d) PL, TRPL spectra and electric field distribution simulated for both structures. e) Energy band diagrams before and after graphene contact with QDs.

18638899, 2025, 20, Downloaded from https://onlinelibrary.wiley.com/doi/10.1002/lpor.202500389 by States Beredning, Wiley Online Library on [05/11/2025]. See the Terms and Conditions (https://onlinelibrary.wiley.com/terms-and-conditions) on Wiley Online Library for rules of use; OA articles are governed by the applicable Creative Commons

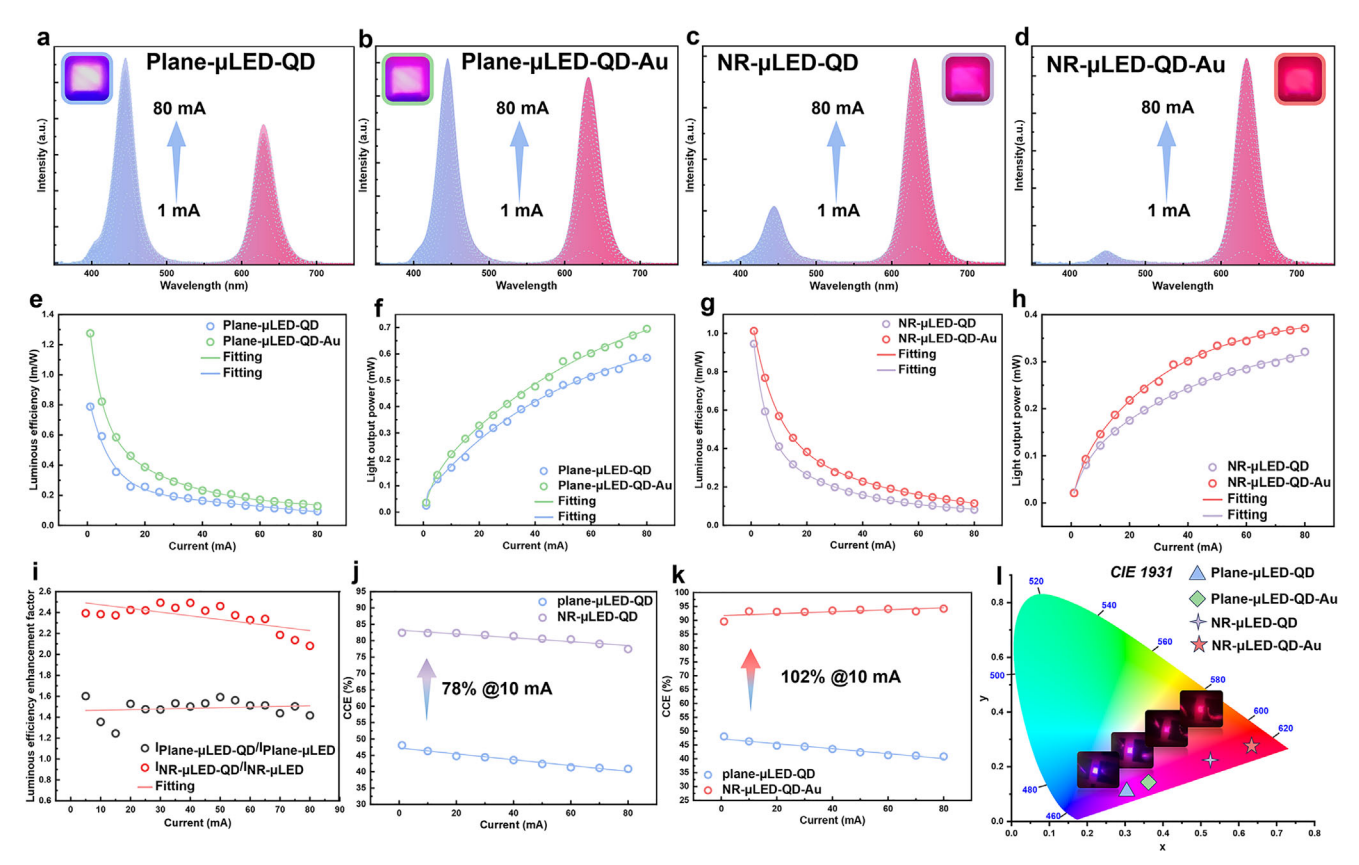


Figure 7. a–d) EL spectra of four μLEDs with planar/nanorod structures and with/without AuNNPs under 1–80 mA current. e–h) Comparison of luminous efficiency and light output power of planar structure μLEDs and nanorod structure μLEDs. i) Enhancement factor of luminous efficiency (IμLED-QD/IμLED) for NR-μLED and plane-μLED with and without QDs. j) Comparison of CCE between planar and nanorod μLEDs (without AuNNPs). k) Comparison of CCE between NR-μLED and plane-μLED after adding AuNNPs. l) Comparison of CIE 1931 chromaticity coordinates for the four μLED structures.

recombination rate is positively correlated with the carrier concentration. The transfer of photoexcited carriers from graphene into the QDs leads to an increase in carrier density within the QDs, thereby enhancing their radiative recombination efficiency and leading to a higher PL intensity. Thus, in addition to serving as a transparent conductive layer to connect individual nanorods, graphene also functions as an electron and hole transport layer. This dual role enhances carrier injection into the QDs and promotes radiative recombination within the QDs, ultimately improving their PL performance.

We conducted optical performance measures on the fabricated planar and nanorod-structured µLEDs. Figure 7a–d shows the EL spectra of the four µLEDs, with the variables being the presence or absence of the nanorod structure and AuNNPs. It is evident that the red-light peak of NR-µLED is significantly higher than the blue light peak, while the red-light peak of Plane-µLED is lower than the blue light peak. This clearly demonstrates the significant role of the nanorod structure in the color conversion. There are two main reasons for this: 1. The QDs enter the nanorod gaps, reducing the distance between the QD and the QW, allowing the QDs to more efficiently absorb the photon energy emitted by the QW; 2. When the distance between the QD and QW is less than 10 nm, a large number of QDs participate in NRET, which directly and effectively improves the energy utilization efficiency of

the QW. In addition to the nanorod structure's ability to enhance CCE, AuNNPs also provide significant assistance, with the LSPR process induced by AuNNPs showing clear benefits in both planar and nanorod structures. From the comparison of the luminous efficiency and light output power of Plane-µLED and NRμLED shown in Figure 7e-h, The data indicate that the samples with AuNNPs outperform the samples without AuNNPs in these two parameters under the same structure. This is due to the enhancement of carrier recombination efficiency inside the QDs by LSPR, leading to increased light emission intensity. By comparing the enhancement factors of luminous efficiency in NRμLED and Plane-μLED with and without QDs, it is apparent that the nanorod structure has a more significant effect on luminous efficiency improvement, as shown in Figure 7i. This is because NRET enhances the energy utilization efficiency of carriers in the QW, reducing non-radiative recombination losses in the QD and allowing more high-frequency photon energy to be converted into low-frequency photons energy. The µLED-QD's CCE can be calculated using the Equation (3):[31,22,43]

$$\eta_{CCE} = \frac{\int_{QD_{emission}} \left(\frac{\lambda}{hc}\right) \times \left[I_{QD}(\lambda)\right] d\lambda}{\int_{QW.\ QD_{emission}} \left(\frac{\lambda}{hc}\right) \times \left[I_{QW}(\lambda) + I_{QD}(\lambda)\right] d\lambda}$$
(3)

www.advancedsciencenews.com

& PHOTONICS REVIEWS

www.lpr-journal.org

Ni surface as a surrent enreading layer. The basis structure of the

where I_{QD} and I_{QW} are the emission intensities of the QD and QW in the EL spectrum. The calculated CCE values for Plane- μ LED-QD and NR- μ LED-QD are shown in Figure 7j. The NRET mechanism and graphene's charge carrier transfer mechanism lead to a CCE of 82% for the graphene-connected nanorod NR- μ LED-QD at 10 mA, representing a 78% improvement over the conventional Plane- μ LED-QD. The LSPR process introduced by AuNNPs significantly enhances the QD's emission intensity and quantum yield. As shown in Figure 7k, the CCE of NR- μ LED-QD-Au reaches 95%, a 102% increase over the Plane- μ LED-QD. In the CIE1931 chromaticity diagram shown in Figure 7l, significant color differences among the four structures are evident. The NR- μ LED-QD-Au design achieves nearly pure red emission, which will be highly beneficial for QD-based μ LED full-color displays.

In addition to the four device structures mentioned above, we also designed four other $\mu LEDs$ with nanorod structures, as shown in Figure S8 (Supporting Information), to explore the effects of the graphene insertion layer, and the presence of a second layer of QDs on the device's CCE. By comparing the optical performance of these NR- $\mu LEDs$ (Figures S9 and S10, Supporting Information), we have reason to believe that the improvement in CCE of the nanorod structure with a graphene insertion layer is not only due to the increase in the number of QDs, but more importantly, because the nanorod structure significantly reduces the distance between the QD and QW. This, in turn, enhances the absorption of radiative energy and introduce NRET, collectively boosting the CCE.

3. Conclusion

In conclusion, we fabricated µLEDs by etching optimized nanorod arrays on the light-emitting mesa, using graphene as a transparent conductive layer to connect the nanorods. The QD/AuNNP mixture was spin-coated into the nanorod gaps, and a second layer of QD/AuNNP mixture was spin-coated on top of the graphene. The nanorod structure significantly reduced the distance between the QDs and QWs, introducing the NRET mechanism, which greatly improved the efficiency of energy utilization. Furthermore, the AuNNPS enhanced the radiative recombination efficiency within QDs through the LSPR effect, boosting the emission intensity of QDs. Finally, graphene in our design not only serves as a transparent conductive layer connecting the individual nanorods but also acts as a carrier transport layer, providing photogenerated carriers to the QDs and enhancing the radiative recombination inside the QDs, ultimately increasing the quantum yield. Combining these physical mechanisms, the CCE of the designed NR-µLED-QD-Au can reach up to 94%, an increase of over 102% compared to the conventional planar design. This work provides a promising strategy for leveraging nanostructures and nanomaterials to realize next-generation full-color µLED displays.

4. Experimental Section

Figure 1 shows the schematic diagram of the fabrication process. We used commercially available GaN-based LED epitaxial wafers on sapphire substrates. To ensure good ohmic contact between the metal electrode and P-GaN, a 110 nm layer of indium tin oxide (ITO) was sputtered onto

the P-GaN surface as a current spreading layer. The basic structure of the final epitaxial structure is shown in Figure 1a. We used photolithography, inductively coupled plasma chemical vapor deposition (ICPCVD), and liftoff techniques to pattern a 300 nm layer of SiO₂ as an etching mask. Then, an inductively coupled plasma reactive ion etching (ICP-RIE) process was used to etch a light-emitting mesa with a height of 1.3 µm and dimensions of 50×50 µm. After etching, a layer of SiO₂ was deposited using ICPCVD as a protective layer covering the entire epitaxial wafer, leaving only a $40 \times 40 \,\mu m$ area exposed on the mesa as the nanorod etching region. Next, using the dip-coating method, we self-assembled a layer of SiO₂ nanospheres, each with a diameter of 800 nm, onto the epitaxial wafer. These SiO₂ nanospheres were then pre-etched for 300 s using reactive ion etching (RIE) (etching gas: CHF3, flow rate: 100 sccm, radio frequency power: 300 W). The pre-etched SiO2 layer served as an etching hard mask to form the nanorods array on the light-emitting mesa via ICP-RIE, with the nanorods achieving a height of 1.3 µm and a diameter of 500 nm. Since the SiO₂ nanospheres acted as an etching mask, we could directly control the diameter of the nanorods by adjusting the etching time of the nanospheres. In the supporting information, we provide the fabrication process for nanorod arrays with different sizes, as well as the corresponding optical performance parameters (Figures S1-S3; Table \$1, Supporting Information). After the nanorod array was etched, we used BOE solution to remove the ${\rm SiO_2}$ protective layer and ${\rm SiO_2}$ nanospheres. Then, we soaked the sample in a 70 °C KOH solution for 5 min to eliminate the sidewall damage introduced during the dry etching process. Next, a 300 nm layer of SiO₂ was deposited using ICPCVD as a sidewall passivation layer and P electrode isolation layer. Finally, a 15/300 nm Ti/Au layer was magnetron sputtered as the P/N electrodes, completing the NR-uLED fabrication in this study. We then used spin-coating to fill the nanorod gaps with a QD/AuNNP mixture. After cleaning the top of the nanorods, we transferred two layers of monolayer graphene onto the top of the nanorod array to connect the individual nanorods. After the graphene transfer, the band bending effect of graphene and QDs is leveraged, along with the mechanical strength of graphene, to use it as both a support layer and an inserted carrier transport layer. A second layer of QD/AuNNP mixture was integrated onto its surface, which effectively collects and utilizes the blue photons escaping from the top of the nanorods, thereby maximizing the CCE. Figure 1i is a schematic of the final device, and Figure 1j shows a cross-sectional view of the device as well as a structural diagram of a single nanorod.

Spin-coating of QD/AuNNPs (process schematic can be seen in Figure S5, Supporting Information): In a stationary state, the mixed solution of QDs and NPs is dropped onto the epitaxial wafer surface. The wafer is first rotated at 500 rpm for 1 min, allowing gravity and centrifugal force to help the QDs/AuNNPs fill the nanorod gaps uniformly. Then, the speed is increased to 1000 rpm and rotated for 30 s to reduce the thickness of the QDs/AuNNPs solution on the wafer surface and ensure the uniform filling of QDs/AuNNPs into the nanorod gaps. Finally, the wafer is rotated at 2000 rpm for 30 s to remove the excess QD/AuNNPs solution on the surface. The wafer is then placed in a drying oven at 60 °C for 1 min to thoroughly dry the QDs/AuNNPs solution. Afterward, a cotton swab dipped in alcohol is used to gently wipe off any residual QDs/AuNNPs on the wafer surface, preventing the graphene from being electrically disconnected from the nanorods in subsequent steps.

Graphene Transfer (process schematic can be seen in Figure S6, Supporting Information): The commercially purchased monolayer graphene is first cut into pieces, with a structure of PMMA/graphene/Cu/graphene/PMMA. O₂ Plasma cleaning is then used to remove the graphene/PMMA layer from the copper foil's backside. The copper foil, which has graphene grown on it, is floated with the graphene side facing upwards in a copper etching solution (CuSO₄: HCI: H₂O = 10 g:50 ml:50 ml). After 2 h of etching, the copper substrate is completely dissolved, leaving the graphene and PMMA support layer floating on the surface of the etching solution. The graphene/PMMA is then picked up using a clean silicon wafer and transferred into deionized water. The wafer is repeatedly transferred back and forth in a container of deionized water for more than 10 cycles to ensure that no excess impurities remain on the graphene surface. After this, the prepared

NR-µLED substrate is used to pick up the graphene/PMMA layer. Once air-dried, the graphene firmly adheres to the NR-μLED surface through van der Waals forces, while surface tension also helps to promote the adhesion. The substrate is then gently immersed in acetone to remove the PMMA support layer, leaving only the graphene on the device surface. The residual acetone is treated with isopropyl alcohol, and after soaking in deionized water, the graphene-covered NR-µLED device is left to naturally air dry at room temperature. Once dried, the same process is repeated to transfer a second layer of graphene onto the nanorod surface. The final step involves photolithography to etch away the unwanted graphene, leaving only the graphene layer at the top of the NR-µLED mesa as the transparent conductive layer. The purpose of using two layers of graphene is to enhance the mechanical strength of the graphene layer and prevent damage to the graphene during the first transfer or growth process. In the supporting information, we show the SEM images of the nanorod surface after transferring graphene once and twice, along with the corresponding atomic force microscopy (AFM) images, transmittance and Raman spectra of the graphene, (Figure S7, Supporting Information). When graphene is transferred once, some damage occurs during transfer process or the graphene growth process, which can affect the conductivity of the nanorods. After transferring graphene twice, although there is a slight decrease in the Raman spectrum and transmittance due to increased thickness and roughness, the continuity of graphene on the nanorod surface has significantly improved. We believe that the two-step graphene transfer method we presented could contribute to achieving high-performance electrical performance in NR-µLEDs.

Supporting Information

Supporting Information is available from the Wiley Online Library or from

Acknowledgements

A.F. and Q.L. contributed equally to this work. The authors thank the support from the National Key Research and Development Program of China (2023YFB3608703 and 2023YFB3608700), the National Natural Science Foundation of China (12474066), the Fujian Science & Technology Innovation Laboratory for Optoelectronic Information of China (2021ZZ122 and 2020ZZ110), the Fujian provincial project (2021HZ0114 and 2024J011312), and Wuhan municipal project (2024010702020024).

Conflict of Interest

The authors declare no conflict of interest.

Data Availability Statement

The data that support the findings of this study are available from the corresponding author upon reasonable request.

Keywords

graphene, local surface plasmon, micro-LED, non-radiative energy, quantum dot

Received: February 20, 2025 Revised: May 6, 2025 Published online: June 6, 2025

[1] T.-Y. Lee, L.-Y. Chen, Y.-Y. Lo, S. Sudheendran Swayamprabha, A. Kumar, Y.-M. Huang, S.-C. Chen, H.-W. Zan, F.-C. Chen, R.-H. Horng, H.-C. Kuo, ACS Photonics 2022, 9, 2905.

- [2] J.-E. Ryu, S. Park, Y. Park, S.-W. Ryu, K. Hwang, H. W. Jang, Adv. Mater. 2023, 35, 2204947.
- [3] X. Fan, T. Wu, B. Liu, R. Zhang, H.-C. Kuo, Z. Chen, Opto-Electron Adv. 2021, 4, 210022.
- [4] X. Zhou, P. Tian, C.-W. Sher, J. Wu, H. Liu, R. Liu, H.-C. Kuo, Prog. Quantum Electron. 2020, 71, 100263.
- [5] A. Gaurav, C.-Y. Tsai, G.-W. Wang, H.-Y. Tsai, Z. Ting Ye, C.-F. Lin, Photon. Res. 2023, 11, 925.
- [6] H. Lu, W. Guo, C. Su, X. Li, Y. Lu, Z. Chen, Z. Lihong, IEEE J. Electron Devices Soc. 2020, 8, 554.
- [7] Y. Gong, Z. Gong, Adv. Mater. Technol. 2023, 8, 2200949.
- [8] J. Shin, H. Kim, S. Sundaram, J. Jeong, B.-I. Park, C. S. Chang, J. Choi, T. Kim, M. Saravanapavanantham, K. Lu, S. Kim, J. M. Suh, K. S. Kim, M.-K. Song, Y. Liu, K. Qiao, J. H. Kim, Y. Kim, J.-H. Kang, J. Kim, D. Lee, J. Lee, J. S. Kim, H. E. Lee, H. Yeon, H. S. Kum, S.-H. Bae, V. Bulovic, K. J. Yu, K. Lee, et al., Nature 2023, 614, 81.
- [9] C.-M. Kang, J.-Y. Lee, D.-J. Kong, J.-P. Shim, S. Kim, S.-H. Mun, S.-Y. Choi, M.-D. Park, J. Kim, D.-S. Lee, ACS Photonics 2018, 5, 4413.
- [10] C.-M. Kang, D.-J. Kong, J.-P. Shim, S. Kim, S.-B. Choi, J.-Y. Lee, J.-H. Min, D.-J. Seo, S.-Y. Choi, D.-S. Lee, *Opt. Express* 2017, 25, 2489.
- [11] Y. Guo, J. Yu, L. Huang, Z. Liu, Z. Gai, T. Zhi, Y. Zhou, T. Tao, B. Liu, R. Zhang, Y. Zheng, Opt. Express 2024, 32, 27662.
- [12] L. Qi, X. Zhang, Photon. Res. 2023, 11, 109.
- [13] T. Ma, J. Chen, Z. Chen, L. Liang, J. Hu, W. Shen, Z. Li, H. Zeng, Adv. Mater. Technol. 2023, 8, 2200632.
- [14] F. Xu, T. Tao, D. Zhang, Y. Zhang, Y. Sang, J. Yu, T. Zhi, Z. Zhuang, Z. Xie, R. Zhang, B. Liu, IEEE Electron Device Lett. 2023, 44, 1320.
- [15] J. Bae, Y. Shin, H. Yoo, Y. Choi, J. Lim, D. Jeon, I. Kim, M. Han, S. Lee, Nat. Commun. 2022, 13, 1862.
- [16] G. Li, M.-C. Tseng, Y. Chen, F. S.-Y. Yeung, H. He, Y. Cheng, J. Cai, E. Chen, H.-S. Kwok, Light Sci. Appl. 2024, 13, 301.
- [17] J. Jang, H. Cho, S. Choi, H. Jeon, C.-m. Kang, Y. Kim, H. Kang, D. Hahm, J. S. Kim, J. H. Jeong, J. A. Kim, W. Choi, S.-Y. Cho, W.-B. Jung, D. Y. Jeon, H.-M. Youn, N. S. Cho, H.-T. Jung, Adv. Opt. Mater. 2024, 13, 2402147.
- [18] D. Yokota, H. Abe, S. Saito, K. Yanagihashi, T. Chiba, T. Oto, Appl. Phys. Lett. 2024, 125, 133502.
- [19] B.-R. Hyun, C.-W. Sher, Y.-W. Chang, Y. Lin, Z. Liu, H.-C. Kuo, J. Phys. Chem. Lett. 2021, 12, 6946.
- [20] Y. Lin, W. Huang, M. Zhanghu, Z. Liu, Opt. Express 2023, 31, 31818.
- [21] T.-Y. Lee, W.-C. Miao, Y.-Y. Hung, Y.-H. Bai, P.-T. Chen, W.-T. Huang, K.-A. Chen, C.-C. Lin, F.-C. Chen, Y.-H. Hong, H.-C. Kuo, *Nanomaterials* 2023. 13, 2099.
- [22] Z. Du, D. Li, W. Guo, F. Xiong, P. Tang, X. Zhou, Y. Zhang, T. Guo, Q. Yan, J. Sun, IEEE Electron Device Lett. 2021, 42, 1184.
- [23] Z. Du, K. Wang, J. Sun, W. Guo, C. Wu, C. Lin, Q. Yan, IEEE Trans. Electron Devices 2023, 70, 1156.
- [24] S.-W. Huang Chen, C.-C. Shen, T. Wu, Z.-Y. Liao, L.-F. Chen, J.-R. Zhou, C.-F. Lee, C.-H. Lin, C.-C. Lin, C.-W. Sher, P.-T. Lee, A.-J. Tzou, Z. Chen, H.-C. Kuo, *Photon. Res.* **2019**, *7*, 416.
- [25] C.-H. Chen, S.-Y. Kuo, H.-Y. Feng, Z.-H. Li, S. Yang, S.-H. Wu, H.-Y. Hsieh, Y.-S. Lin, Y.-C. Lee, W.-C. Chen, P.-H. Wu, J.-C. Chen, Y.-Y. Huang, Y.-J. Lu, Y. Kuo, C.-F. Lin, C. C. Yang, *Opt. Express* 2023, 31, 6327.
- [26] Z. Zhuang, X. Guo, B. Liu, F. Hu, Y. Li, T. Tao, J. Dai, T. Zhi, Z. Xie, P. Chen, D. Chen, H. Ge, X. Wang, M. Xiao, Y. Shi, Y. Zheng, R. Zhang, Adv. Funct. Mater. 2016, 26, 36.
- [27] Y.-C. Lai, S. Yang, H.-Y. Feng, Y.-C. Lee, Z.-H. Li, S.-H. Wu, Y.-S. Lin, H.-Y. Hsieh, C.-J. Chu, W.-C. Chen, Y.-Y. Huang, Y. Kuo, C. C. Yang, Opt. Express 2023, 31, 16010.
- [28] Z. Shi, Y. Li, S. Li, X. Li, D. Wu, T. Xu, Y. Tian, Y. Chen, Y. Zhang, B. Zhang, C. Shan, G. Du, Adv. Funct. Mater. 2018, 28, 1707031.

e00389 (10 of 11)



LASER & PHOTONICS REVIEWS

www.lpr-journal.org

www.advancedsciencenews.com

- [29] F. Nan, S. Liang, X.-L. Liu, X.-N. Peng, M. Li, Z.-J. Yang, L. Zhou, Z.-H. Hao, Q.-Q. Wang, Appl. Phys. Lett. 2013, 102, 163112.
- [30] G. Lu, Z. Yang, K. Zheng, S. Lin, J. Liu, B. Ye, J. Huang, Y. Zhang, Y. Ye, T. Guo, G. Chen, Org. Electron. 2020, 77, 105540.
- [31] A. Fang, P. Tang, Y. Xie, Z. Du, W. Guo, Y. Mei, H. Xu, J. Sun, Adv. Optical Mater. 2024, 12, 2400230.
- [32] X. Wang, X. H. Li, C. Jiang, C. T. A. Brown, J. Q. Ning, K. Zhang, Q. Yu, X. T. Ge, Q. J. Wang, Z. Y. Zhang, npj 2D Mater. Appl. 2020, 4, 27
- [33] Q. N. D. Lung, R. J. Chu, Y. Kim, T. Laryn, M. A. Madarang, O. Kovalchuk, Y.-W. Song, I.-H. Lee, C. Choi, W. J. Choi, D. Jung, *Nano Lett.* 2023, 23, 3344.
- [34] M. Huang, P. V. Bakharev, Z.-J. Wang, M. Biswal, Z. Yang, S. Jin, B. Wang, H. J. Park, Y. Li, D. Qu, Y. Kwon, X. Chen, S. H. Lee, M.-G Willinger, W. J. Yoo, Z. Lee, R. S. Ruoff, Nat. Nanotechnol. 2020, 15, 289.
- [35] Y. Mei, M. Xie, T. Yang, X. Hou, W. Ou, H. Long, L. Ying, Y. Liu, G. Weng, S. Chen, B. Zhang, ACS Photonics 2022, 9, 3967.

- [36] G. Traetta, A. Di Carlo, A. Reale, P. Lugli, M. Lomascolo, A. Passaseo, R. Cingolani, A. Bonfiglio, M. Berti, E. Napolitani, M. Natali, S. K. Sinha, A. V. Drigo, J. Cryst. Growth 2001, 230, 492.
- [37] N. Anand, D. Kumar Ghosh, A. Abbes, M. Kundu, Md. A. Rahman, C. G. Jenson, R. Morandotti, Md. Zunaid Baten, S. Md, ACS Nano 2024, 18, 26882.
- [38] S.-W. Wang, K.-B. Hong, Y.-L. Tsai, C.-H. Teng, A.-J. Tzou, Y.-C. Chu, P.-T. Lee, P.-C. Ku, C.-C. Lin, H.-C. Kuo, Sci. Rep. 2017, 7, 42962.
- [39] X. Zhang, H. Hu, Y. Qie, L. Lin, T. Guo, F. Li, ACS Appl. Mater. Interfaces 2024, 16, 13219.
- [40] H. Y. Lin, Y. F. Chen, J. G. Wu, D. I. Wang, C. C. Chen, Appl. Phys. Lett. 2006, 88, 161911.
- [41] S. N. Sharma, Z. S. Pillai, P. V. Kamat, J. Phys. Chem. B 2003, 107, 10088.
- [42] S. Chanyawadee, P. G. Lagoudakis, R. T. Harley, M. D. B. Charlton, D. V. Talapin, H. W. Huang, C.-H. Lin, Adv. Mater. 2010, 22, 602.
- [43] Y.-M. Huang, J.-H. Chen, Y.-H. Liou, K. J. Singh, W.-C. Tsai, J. Han, C.-J. Lin, T.-S. Kao, C.-C. Lin, S.-C. Chen, *Nanomaterials* 2021, 11, 2696.